

Graphene as a Lattice Field Theory

Simon Hands*

*Department of Physics, College of Science, Swansea University,
Singleton Park, Swansea SA2 8PP, U.K.*

E-mail: s.hands@swan.ac.uk

Wes Armour

*Oxford e-Research Centre, University of Oxford,
7 Keble Road, Oxford OX1 3QG, U.K.*

E-mail: wes.armour@oerc.ox.ac.uk

Costas Strouthos

*School of Sciences, Department of Computer Science, European University Cyprus,
1516 Cyprus.*

E-mail: Strouthos@ucy.ac.cy

We introduce effective field theories for the electronic properties of graphene in terms of relativistic fermions propagating in 2+1 dimensions, and outline how strong inter-electron interactions may be modelled by numerical simulation of a lattice field theory. For strong enough coupling an insulating state can form via condensation of particle-hole pairs, and it is demonstrated that this is a theoretical possibility for monolayer graphene. For bilayer graphene the effect of an interlayer bias voltage can be modelled by the introduction of a chemical potential (akin to isospin chemical potential in QCD) with no accompanying sign problem; simulations reveal the presence of strong interactions among the residual degrees of freedom at the resulting Fermi surface, which is disrupted by an excitonic condensate. We also present preliminary results for the quasiparticle dispersion, which permit direct estimates of both the Fermi momentum k_F and the induced gap Δ .

*9th International Workshop on Critical Point and Onset of Deconfinement - CPOD2014,
17-21 November 2014
ZiF (Center of Interdisciplinary Research), University of Bielefeld, Germany*

*Speaker.

In this talk I will discuss an effective field theory for electron excitations in graphene, and show how it may be approached using the same lattice field theory methods more usually applied to the strong interaction between quarks and gluons. I will argue that for sufficiently strong inter-electron coupling, of the same order as that found in suspended graphene samples, there is a phase transition to an insulating phase, described by a quantum critical point (QCP). I will then specialise to the case of bilayer graphene with a biasing voltage applied between the layers, so that there is a non-zero density of electrons on one layer and holes on the other. This is formally very similar to the case of non-zero chemical potential for isospin in QCD, and will permit numerical simulations probing degenerate matter (albeit in $2+1d$) in the presence of strong interactions.

1. Relativity in Graphene

Let's begin with a simple tight-binding model, with a Hamiltonian describing electrons in π -orbitals hopping between A and B sublattices on the bipartite honeycomb lattice appropriate for a graphene monolayer (an excellent introduction can be found in the review by Castro Neto *et al* [1]):

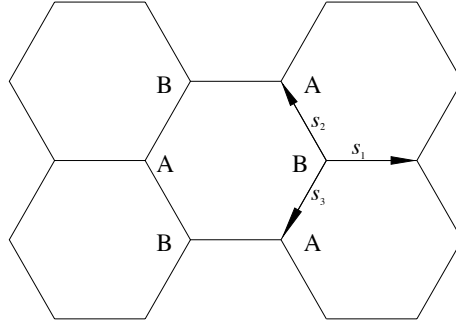


Figure 1: The honeycomb lattice of monolayer graphene.

$$H = -t \sum_{\vec{r} \in B} \sum_{i=1}^3 b^\dagger(\vec{r}) a(\vec{r} + \vec{s}_i) + a^\dagger(\vec{r} + \vec{s}_i) b(\vec{r}) \quad (1.1)$$

In momentum space the Hamiltonian is rewritten

$$H = \sum_{\vec{k}} \left(\Phi(\vec{k}) a^\dagger(\vec{k}) b(\vec{k}) + \Phi^*(\vec{k}) b^\dagger(\vec{k}) a(\vec{k}) \right) \text{ with } \Phi(\vec{k}) = -t \left[e^{ik_x l} + 2 \cos\left(\frac{\sqrt{3}k_y l}{2}\right) e^{-i\frac{k_x l}{2}} \right] \quad (1.2)$$

where l is the length of a CC bond. Notice how the fact that a link emerging from a site is not matched by another leaving at 180° results in a complex-valued kernel $\Phi(\vec{k})$. If we define states $|\vec{k}_\pm\rangle = (\sqrt{2})^{-1} [a^\dagger(\vec{k}) \pm b^\dagger(\vec{k})] |0\rangle$, then

$$\langle \vec{k}_\pm | H | \vec{k}_\pm \rangle = \pm (\Phi(\vec{k}) + \Phi^*(\vec{k})) \equiv \pm E(\vec{k}), \quad (1.3)$$

so that the energy spectrum is symmetric about $E = 0$.

In fact, $E = 0$ at precisely two independent points within the first Brillouin Zone, the so-called *Dirac points* $\vec{k} = \vec{K}_\pm = (0, \pm 4\pi/3\sqrt{3}l)$. Linearise about these points;

$$\Phi(\vec{K}_\pm + \vec{p}) = \pm v_F [p_y \pm ip_x] + O(p^2) \text{ with } v_F = \frac{3}{2}tl. \quad (1.4)$$

The Fermi velocity $v_F \approx 10^6 \text{ms}^{-1}$ in graphene. Now define modified electron operators $a_\pm(\vec{p}) = a(\vec{K}_\pm + \vec{p})$ etc, and combine them into a four-spinor $\Psi = (b_+, a_+, a_-, b_-)^T$. To linear order in p the complex structure implicit in (1.4) results in the Dirac Hamiltonian

$$H = v_F \sum_{\vec{p}} \Psi^\dagger(\vec{p}) \vec{\alpha} \cdot \vec{p} \Psi(\vec{p}), \quad (1.5)$$

with 4×4 matrices obeying $\{\alpha_i, \alpha_j\} = \delta_{ij}$. In other words, low-energy excitations in graphene are massless relativistic fermions with velocity $\approx c/300$. For monolayer graphene, the number of relativistic flavors $N_f = 2$, ie 8 spinor degrees of freedom = 2 C atoms/unit cell \times 2 Dirac points \times 2 spins.

Electron-electron interactions in graphene can't be ignored for two reasons. Firstly, Debye screening is suppressed due to the vanishing density of free electron states at the Dirac points. Secondly, the effective fine structure constant is boosted by a factor c/v_F and is hence of order unity. The following effective field theory treats interactions in a simple way [2, 3]:

$$S = \sum_{a=1}^{N_f} \int dx_0 d^2x (\bar{\psi}_a \gamma_0 \partial_0 \psi_a + v_F \bar{\psi}_a \vec{\gamma} \cdot \vec{\nabla} \psi_a + iV \bar{\psi}_a \gamma_0 \psi_a) + \frac{1}{2e^2} \int dx_0 d^3x (\partial_i V)^2. \quad (1.6)$$

The field V is an ‘‘instantaneous’’ Coulomb potential governed by 3d Maxwell electrodynamics with $v_F \ll c$, interacting with relativistic electrons moving in the plane; this is a ‘‘braneworld’’. In the large- N_f limit the V -propagator is given by

$$D(p) = \left(\frac{2|\vec{p}|}{e^2} + \frac{N_f}{8} \frac{|\vec{p}|^2}{(p_0^2 + v_F^2 |\vec{p}|^2)^{\frac{1}{2}}} \right)^{-1}. \quad (1.7)$$

The first term is the classical result, the second is the leading quantum correction arising from vacuum polarisation due to virtual electron-hole pairs. In the static limit $p_0 = 0$ both contributions yield a $1/r$ potential. The dimensionless combination $\lambda = e^2 N_f / 16\epsilon \epsilon_0 \hbar v_F \simeq 1.4 N_f / \epsilon$ parametrises the relative strengths of quantum vs. classical, and depends on the dielectric constant ϵ of the substrate on which the graphene sits. λ is maximal for ‘‘suspended’’ graphene for which $\epsilon = 1$.

For sufficiently large e^2/ϵ or sufficiently small N_f it has been hypothesised that the Fock vacuum is unstable with respect to condensation of particle-hole pairs with $\langle \bar{\psi} \psi \rangle \neq 0$, spontaneously breaking the global $U(2N_f)$ symmetry of (1.6) to $U(N_f) \otimes U(N_f)$ and leading to a gapping of the electron dispersion at the Dirac points [3]. In particle physics we say a fermion mass is dynamically generated via a chiral condensate; in condensed matter physics the resulting phase is known as a *Mott insulator*. The transition occurring at $e_c^2(N_f)$ defines a QCP whose universal properties characterise the low-energy excitations of graphene. In the (e^2, N_f) plane the QCPs lie along a

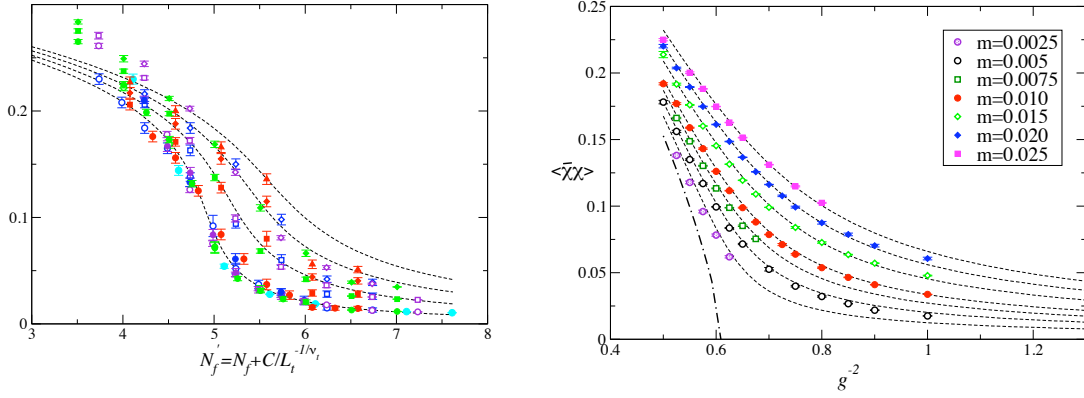


Figure 2: Chiral order parameter $\langle \bar{\chi} \chi \rangle$ resulting from (2.1) for various m at strong coupling (left), and for $N_f = 2$ (right).

phase boundary between insulating and metallic phases, and the values of exponents such as δ in the critical scaling relation

$$\langle \bar{\psi} \psi \rangle|_{e^2=e_c^2} \propto m^{\frac{1}{\delta}}, \quad (1.8)$$

where m is an explicit symmetry-breaking mass parameter, depend on N_f . This behaviour is similar to that of the $3d$ Thirring model, whose phase diagram has been mapped numerically over many years [4], and inspires a treatment based on the technically simpler action (with units $v_F = 1$)

$$S = \sum_{a=1}^{N_f} \int dx_0 d^2x \left[\bar{\psi}_a \gamma_\mu \partial_\mu \psi_a + iV \bar{\psi}_a \gamma_0 \psi_a + \frac{1}{2g^2} V^2 \right] \quad (1.9)$$

This has the identical $D(p)$ in the strong-coupling limit, but the Coulombic r^{-1} tail is screened for $g^2 < \infty$. The relation between g^2 and e^2, λ is not known *a priori*.

2. Lattice Approach

Due to the absence of small parameters at the QCP, a non-perturbative approach is needed. We have used a lattice model based on the staggered fermion formulation on a cubic lattice, with action ($i = 1, \dots, N$) [5]

$$S_{latt} = \frac{1}{2} \sum_{x\mu i} \bar{\chi}_x^i \eta_{\mu x} (1 + i\delta_{\mu 0} V_x) \chi_{x+\hat{\mu}}^i - \bar{\chi}_x^i \eta_{\mu x} (1 - i\delta_{\mu 0} V_{x-\hat{0}}) \chi_{x-\hat{\mu}}^i + m \sum_{xi} \bar{\chi}_x^i \chi_x^i + \frac{N}{4g^2} \sum_x V_x^2 \quad (2.1)$$

The fermion fields $\chi, \bar{\chi}$ are defined on lattice sites, and the boson fields V on the timelike links. The sign factors $\eta_{\mu x} \equiv (-1)^{x_0 + \dots + x_{\mu-1}}$ ensure a covariant continuum limit in the free-field limit $g^2 = 0$. The action (2.1) only has a chance of recovering the physics of (1.6) at a QCP, where for instance details of the underlying lattice should become irrelevant. However, (2.1) exhibits a distinct chiral symmetry breaking pattern $U(N) \otimes U(N) \rightarrow U(N)$; away from weak coupling, there is no guarantee of “taste symmetry restoration” ensuring the correct continuum symmetries with $N_f = 2N$.

Fig. 2 shows the order parameter $\langle \bar{\chi} \chi(m) \rangle$ as a function of N_f in the strong coupling limit (left) [5], and as a function of g^{-2} for the monolayer value $N_f = 2$ (right) [6]. In both cases a power-law equation of state appropriate for a continuous phase transition has been fitted; this identifies the location of the QCP. The left hand plot shows a critical value $N_{fc} = 4.8(2)$, proving that a QCP exists for finite g^2 for $N_f = 2 < N_{fc}$, and is thus potentially relevant for monolayer graphene. The right hand plot shows a critical coupling $g_c^{-2} = 0.609(2)$ for $N_f = 2$, with the critical exponent $\delta = 2.66(3)$, to be contrasted with $\delta(N_{fc}) = 5.5(3)$. The model (2.1) has also been used to study the symmetry restoring transition at temperature $T > 0$, expected to be of BKT type [7].

These results are consistent with those obtained by simulating the braneworld gauge theory [8]. That work initially suggested the QCP might occur at a coupling sufficiently small that suspended graphene samples might lie in the insulating phase. Later simulations on a $2d$ honeycomb lattice with a more realistic inter-electron potential suggest the critical coupling is slightly too strong for a Mott insulator to be observed, although modification of the electron dispersion in pure suspended samples due to the vicinity of a QCP is not excluded [9].

3. Bilayer Graphene

There is just as much interest in graphene samples formed from two honeycomb layers, in which the A atoms of one sheet lie directly over the B atoms of its neighbour. Naively, electron transport should have an effective description with $N_f = 4$ relativistic fermions; however in the absence of any further interactions the Hamiltonian (1.1) actually predicts a parabolic band structure [10]. Let's rename the original intralayer coupling along a CC bond within a layer t_0 and introduce new interlayer couplings t_1 between overlying AB sites and t_3 between AB sites displaced horizontally a distance l . This latter coupling results in a trigonal distortion of the parabolic band, breaking it into four separate cones at the Dirac point. It turns out an $N_f = 4$ effective field theory description is plausible for long-wavelength excitations with $kl \lesssim t_1 t_3 / t_0^2$.

The new ingredient in the bilayer problem is the possibility of applying a bias voltage across the layers, inducing a negative charge on one layer due to non-zero density of electrons, and a positive charge on the other due to holes. Denoting this voltage by 2μ we can introduce it with positive minimal coupling to fields ψ on the the upper layer and negative coupling to fields ϕ on the lower. This is formally identical to the introduction of an isospin chemical potential in two-flavor QCD. The lagrangian density in continuum notation reads [11]

$$\mathcal{L} = (\bar{\psi}, \bar{\phi}) \begin{pmatrix} D[V; \mu] + m & ij \\ -ij & D[V; -\mu] - m \end{pmatrix} \begin{pmatrix} \psi \\ \phi \end{pmatrix} + \frac{1}{2g^2} V^2 \equiv \bar{\Psi} \mathcal{M} \Psi + \frac{1}{2g^2} V^2, \quad (3.1)$$

where $D[V; \mu] = D[V; 0] + \mu \gamma_0 = -D^\dagger[V; -\mu]$. The parameter m is a symmetry-breaking gap parameter due to intralayer particle-hole pairing, and j a gap parameter due to interlayer pairing; the bound state formed in the latter case is known as an *exciton*. They act as IR regulators for the model; in practice numerical simulations with $m = 0$, $j \neq 0$ are perfectly feasible. The model is not realistic in the sense that intralayer $\psi - \psi$ interactions have the same coupling strength as interlayer $\psi - \phi$; however, from a simulator's point of view the key feature is the identity

$$\det \mathcal{M} = \det[(D + m)^\dagger (D + m) + j^2] > 0. \quad (3.2)$$

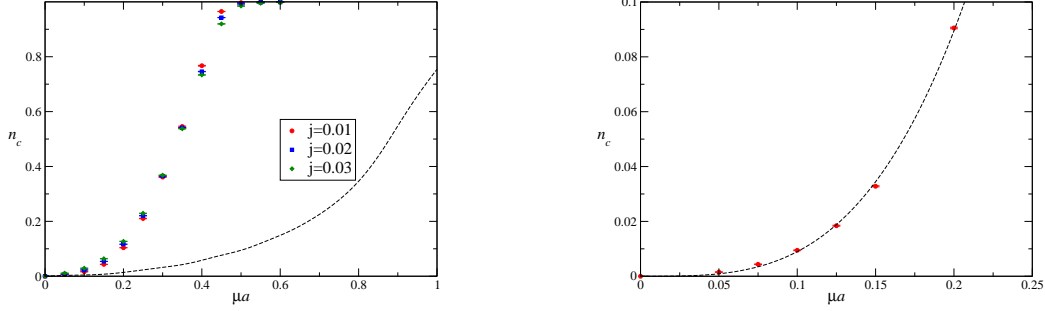


Figure 3: Carrier density n_c in bilayer model as a function of μ (left), and in the small μ $j \rightarrow 0$ limit (right).

Even with $\mu \neq 0$ the model has no sign problem and is amenable to orthodox Monte Carlo methods.

We have implemented a lattice version of (3.1) using $N = 2$ staggered fermion flavors on 32^3 and 48^3 lattices. Since $N_f = 4$ is close to N_{fc} , it is hard to identify the location of the QCP; we set $(g^2 a)^{-1} = 0.4^1$, which we believe is just to the sub-critical side of the QCP. Simulations with varying μ have been performed, and the following observables monitored:

$$\text{carrier density } n_c \equiv \frac{\partial \ln \mathcal{Z}}{\partial \mu} = \langle \bar{\psi} D_0 \psi \rangle - \langle \bar{\phi} D_0 \phi \rangle, \quad (3.3)$$

$$\text{exciton condensate } \langle \Psi \Psi \rangle \equiv \frac{\partial \ln \mathcal{Z}}{\partial j} = i \langle \bar{\psi} \phi - \bar{\phi} \psi \rangle, \quad (3.4)$$

$$\text{chiral condensate } \langle \bar{\Psi} \Psi \rangle \equiv \frac{\partial \ln \mathcal{Z}}{\partial m} = \langle \bar{\psi} \psi - \bar{\phi} \phi \rangle. \quad (3.5)$$

The exciton condensate $\langle \Psi \Psi \rangle$ (3.4) caused by spontaneous pairing of electrons and holes between layers is a new feature; just like any other pairing phenomenon it is expected to induce a gap rendering the ground state insulating. By varying μ we can check how exciton condensation varies with the extent of the Fermi surface (strictly a Fermi line in $2+1d$).

Fig. 3 shows simulation results for n_c ; at the left the data rise steeply with μ to reach a plateau at $\mu a \approx 0.5$. There is no discernable onset μ_o below which n_c vanishes. The plateau marks the *saturation region* where the lattice contains one fermion (both particle and hole) per site and the Exclusion Principle prevents further occupation. It should be regarded as an artifact of simulating continuous fields on a discrete lattice. Interestingly, all other known simulable lattice models reach saturation at $\mu a \sim O(1)$; indeed, the result for free fermions in $2+1d$ is shown as a dashed line. In the limit $T \rightarrow 0$, μ coincides with the Fermi energy E_F . Since n_c is directly related to the Fermi momentum k_F , the precocious saturation is the first hint that $E_F < k_F$, ie. the system is strongly self-bound. At right the $j \rightarrow 0$ extrapolated data are fitted to a power law, with the result $n_c(j=0) \propto \mu^{3.32(1)}$. The density rises faster than the free-field expectation $n_c \propto \mu^2$ coming from the area of the Fermi disk.

Fig. 4 shows the corresponding plots for $\langle \Psi \Psi \rangle$. Again there is a steep rise to a peak at $\mu a \approx 0.3$, followed by an even more rapid descent to zero in the saturation region. The free-field results,

¹Care is needed since *a priori* there is no reason for spatial and temporal lattice spacings to coincide at the QCP.

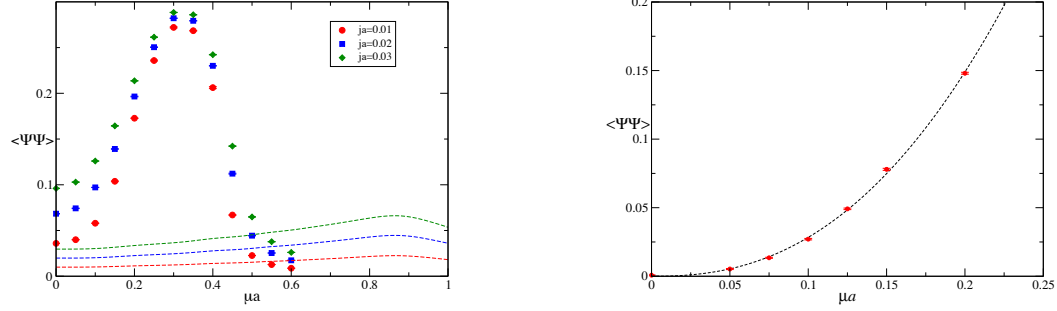


Figure 4: Exciton condensate $\langle\Psi\Psi\rangle$ as a function of μ (left), and in the small $\mu j \rightarrow 0$ limit (right).

which are much smaller and extremely sensitive to j , are shown as dashed lines. The extrapolated data is fitted by $\langle\Psi\Psi(j=0)\rangle \propto \mu^{2.39(2)}$. As we will see below, this result also suggests a weak-coupling approach is not applicable.

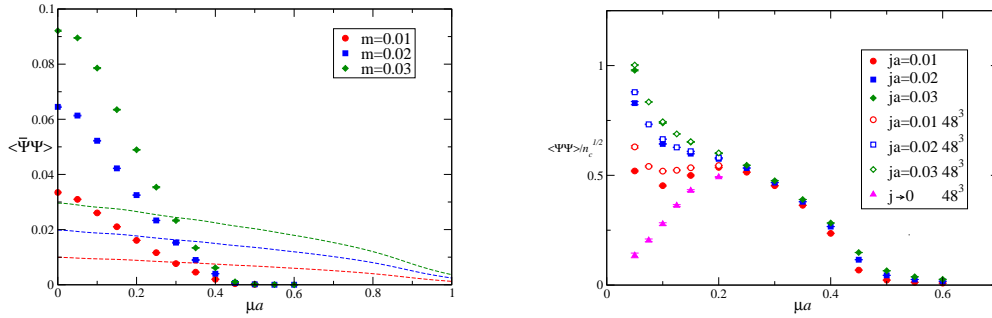


Figure 5: Chiral condensate $\langle\bar{\Psi}\Psi\rangle$ vs. μ (left), and the ratio $\langle\Psi\Psi\rangle/\sqrt{n_c}$ vs. μ for various j (right).

The left panel of Fig. 5 shows the intralayer condensate $\langle\bar{\Psi}\Psi\rangle$; for small μ it exceeds its free-field value, as might be expected from the strong interactions close to a QCP, but then rapidly falls to zero as μ increases, so that by the time $\mu a=0.3$ where $\langle\Psi\Psi\rangle$ peaks, it falls below the free-field value. This can be understood in terms of a competition between the two condensates; intralayer pairing is suppressed as E_F grows, because more energy is needed to excite a particle-hole pair from a single layer, whereas interlayer pairing is enhanced by the larger density of states as k_F grows. Even at $\mu = 0$ $|\langle\bar{\Psi}\Psi\rangle| \approx \frac{1}{3}|\langle\Psi\Psi\rangle|_{peak}$.

Now, $\langle\Psi\Psi\rangle$ is simply the density of exciton pairs in the ground state. In a weakly-coupled BCS picture of exciton condensation, the excitons would be drawn from a shell of thickness Δ around the Fermi surface, where Δ is the induced gap; we would then expect $\langle\Psi\Psi\rangle \propto \Delta k_F \propto \Delta n_c^{\frac{1}{2}}$, where the last step follows from Luttinger's theorem relating n_c to the volume enclosed within the Fermi surface. Thus we predict

$$\Delta(\mu) \propto \frac{\langle\Psi\Psi(\mu)\rangle}{\sqrt{n_c(\mu)}}. \quad (3.6)$$

The quantity on the RHS of (3.6) is plotted as a function of μ in the RH panel of Fig. 5, with particular attention paid to the extrapolation to both thermodynamic and $j \rightarrow 0$ limits. For small μ we infer $\Delta \propto \mu$; at a QCP no other behaviour could arise, since μ is the only scale. This should be contrasted with other models studied using lattice simulation; in the non-renormalisable NJL model, $\Delta \propto \Lambda_{UV}$ [12], whereas in two-color QCD $\Delta = O(\Lambda_{QCD})$ [13]. In neither case is there any significant dependence on μ .

4. Quasiparticle Dispersion in Bilayer Graphene

In order to confirm the picture developed in the previous section of a system with $k_F > \mu$ and $\Delta \propto \mu$ it would clearly help to have direct knowledge of these quantities from the fermion (in this context known as the *quasiparticle*) dispersion relation $E(k)$. Here we present preliminary results obtained from the Euclidean propagator $\langle \Psi(k) \bar{\Psi}(k) \rangle \propto e^{-E(k)t}$ on 32^3 ; to improve momentum resolution partially twisted boundary conditions are used [14], so that the smallest non-zero k is $\pi/48a$. We calculated the timeslice correlators in both normal and anomalous channels according to

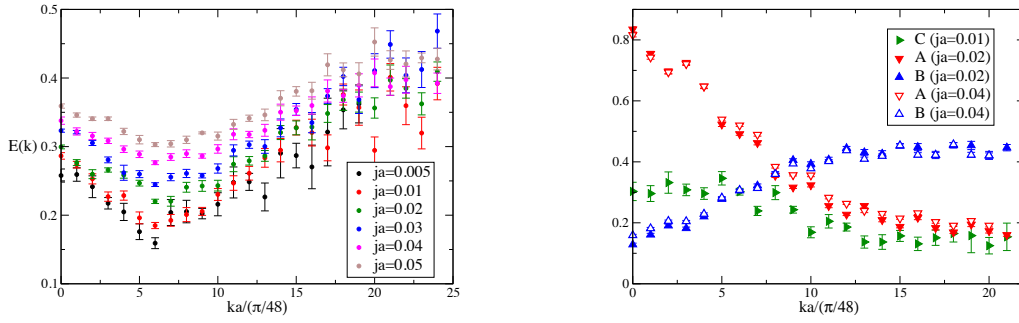


Figure 6: Quasiparticle dispersion relation $E(k)$ at $\mu a = 0.2$ for various j (left), and the fitted propagator amplitudes (right).

$$C_N(\vec{k}, t) = \sum_{\vec{x}} \langle \psi(\vec{0}, 0) \bar{\psi}(\vec{x}, t) \rangle e^{-i\vec{k} \cdot \vec{x}}; \quad C_A(\vec{k}, t) = \sum_{\vec{x}} \langle \psi(\vec{0}, 0) \bar{\phi}(\vec{x}, t) \rangle e^{-i\vec{k} \cdot \vec{x}} \quad (4.1)$$

and fitted to the forms [15].

$$C_N(k, t) = Ae^{-Et} + Be^{-E(L_t - t)}; \quad C_A(k, t) = C(e^{-Et} - e^{-E(L_t - t)}). \quad (4.2)$$

The resulting dispersion $E(k)$ is shown for several j in the left panel of Fig. 6. The clear dip marks the Fermi surface; for $k < k_F$ the correlator is dominated by forwards-propagating holes, and for $k > k_F$ by backwards-propagating particles, as demonstrated in the relative magnitudes of the amplitudes A and B in Fig. 6 (right). Note that the amplitude C for anomalous propagation, in which eg. an electron in one layer is absorbed by an exciton transferring its momentum to an electron in the other, is comparable in magnitude to those for normal propagation for a range of momenta with $k \approx k_F$.

From the plots we estimate $k_F a \approx 0.4 > \mu a = 0.2$, supporting the earlier contention that $k_F > E_F$ due to the self-bound nature of the system near the QCP. As a sanity check we note that for free lattice fermions the carrier density $n_c^{freelatt}(\mu a = 0.4)a^2 \approx 0.06$, to be compared with the directly measured value 0.09 (see Fig. 3).

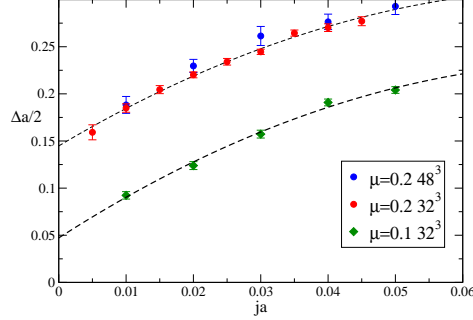


Figure 7: Gap $\Delta(j)$ estimated from the minimum of $E(k)$.

Finally in Fig. 7 we plot the gap Δ estimated from the minima of $E(k)$ in Fig. 6, with data taken at two different values of μ . We can then extrapolate to $j = 0$ and estimate $\Delta a(\mu = 0.1) \approx 0.1$, $\Delta a(\mu = 0.2) \approx 0.3$. This is roughly consistent with our earlier prediction that $\Delta \propto \mu$, and supports a physical picture of a gapped Fermi surface with $\Delta/\mu \sim O(1)$. This should be compared with studies using a diagrammatic approach predicting $\Delta/\mu \sim 10^{-7}$ [16].

5. Summary

We've discussed how the effective description of graphene in terms of relativistic field theory can be studied non-perturbatively using orthodox lattice simulation techniques familiar from particle physics. The simulations have confirmed at least the theoretical possibility of a QCP in monolayer graphene which may have relevance for the correct description of charge transport in suspended samples. In the case of bilayer graphene the model presented here, though arguably not very realistic due to the equality of intra- and inter-layer interaction strengths, is at least an interesting new member of the rather exclusive stable of models which permit study by Monte Carlo techniques in the presence of a chemical potential. As we have seen, its behaviour is rather different from other models in this class (NJL, QC₂D) because residual interactions at the Fermi surface are strong in the vicinity of a QCP.

References

- [1] A.H. Castro Neto, F. Guinea, N.M.R. Peres, K.S. Novoselov and A.. Geim, Rev. Mod. Phys. **81** (2009) 109.
- [2] D.V. Khveshchenko, Phys. Rev. Lett. **87** (2001) 246802.
- [3] D.T. Son, Phys. Rev. B **75** (2007) 235423.

- [4] L. Del Debbio, S.J. Hands and J.C. Mehegan, Nucl. Phys. B **502** (1997) 269; L. Del Debbio and S. J. Hands, Nucl. Phys. B **552** (1999) 339; S. Hands and B. Lucini, Phys. Lett. B **461** (1999) 263; S. Christofi, S. Hands and C. Strouthos, Phys. Rev. D **75** (2007) 101701.
- [5] S.J. Hands and C.G. Strouthos, Phys. Rev. B **78** (2008) 165423.
- [6] W. Armour, S. Hands and C. Strouthos, Phys. Rev. B **81** (2010) 125105.
- [7] W. Armour, S. Hands and C. Strouthos, Phys. Rev. B **84** (2011) 075123.
- [8] J.E. Drut and T.A. Lähde, Phys. Rev. Lett. **102** (2009) 026802; Phys. Rev. B **79** (2009) 165425.
- [9] M.V. Ulybyshev, P.V. Buividovich, M.I. Katsnelson and M.I. Polikarpov, Phys. Rev. Lett. **111** (2013) 056801.
- [10] E. McCann and V.I. Fal'ko, Phys. Rev. Lett. **96** (2006) 086805.
- [11] W. Armour, S. Hands and C. Strouthos, Phys. Rev. D **87** (2013) 6, 065010.
- [12] S. Hands and D. N. Walters, Phys. Rev. D **69** (2004) 076011.
- [13] S. Hands, S. Kim and J.-I. Skullerud, Eur. Phys. J. C **48** (2006) 193; S. Cotter, P. Giudice, S. Hands and J.-I. Skullerud, Phys. Rev. D **87** (2013) 3, 034507.
- [14] J.M. Flynn, A. Jüttner and C.T. Sachrajda, Phys. Lett. B **632** (2006) 313.
- [15] S. Hands, B. Lucini and S. Morrison, Phys. Rev. D **65** (2002) 036004.
- [16] M.Yu. Kharitonov and K.B. Efetov, Semicond. Sci. Technol. **25** (2010) 034004.